

Microplane modeling of the elasto-viscoplastic constitution

Muhammad Saleem*

*Air University Islamabad, Multan campus, Pakistan

ARTICLE INFO

Article history:

Received 25 Apr 2020

Received in revised form 11 June 2020

Accepted 15 July 2020

Keywords:

Constitutive Model, Elasto-viscoplastic,

Microplane, Strain Rate.

ABSTRACT

In this paper, the elasto-viscoplastic Constitutive model is applied within the Microplane framework. The use of strain-dependent models allows measuring the effect of loading speed on the soil. Additionally, rate-based behavior models in simulation modeling avoid the uniqueness of the ruling equation. The proposed model can plot the stress-strain history on plates with different angles inside the soil. Therefore, valuable information can be obtained about the failure plane. Using the Microplane framework enables this hybrid behavior model to predict local strain.

1. INTRODUCTION

Microplane refers to planes within materials that have different angles. This model is used to examine the structure of fine materials. Taylor proposed the original idea for this model and was called Slip Panels (Pham et al, 2011). Taylor's idea was formulated by Roters (2019). Many researchers have used this model to study metals, soils, and rocks.

Before 1984, microscopic Constitutive models were developed on a consistent fixed basis. But proving satisfactory coping conditions was a difficult issue for this Constitutive model. This ambiguity was resolved by Bazant and Gambarova (1984). In this method, instead of the stress tensor image, the strain tensor image is applied to the image planes. As a result, the compatibility condition is fulfilled and the equilibrium conditions are created using the Principle of Virtual Work.

The elasto-viscoplastic Constitutive model identified in this paper was presented by Teichtmeister et al., (2017). This Constitutive model was developed using concepts of critical state and viscoplasticity. The benefits of this Constitutive model include primary and secondary pressure modeling, predicting the effect of stress rate on Untrained shear tests, and creep modeling. In this constitutive model, the elastic strain is considered to be non-rate dependent. An advantage of this assumption is the ease of use of this constitutive model. Besides, the dependence of plastic strain on time seems more rational (Perzyna, 1966; Wu et al., 2018; Diehl et al., 2017).

Microplane modeling of the elasto-viscoplastic behavior, allows us to use the unique features of both models simultaneously. On the one hand, the rate-dependent behavior of the soil is simulated by the elasto-viscoplastic model, and on the other, the behavior of the fine or microstructure is described by the Microplane framework.

1.1. Formulation of elasto-viscoplastic Constitutive model

Teichtmeister et al., (2017) considered the stress rate as two parts of elastic ($\dot{\epsilon}_{ij}^e$) and viscoplastic ($\dot{\epsilon}_{ij}^{vp}$). This model assumes that the strain rate is time-dependent.

$$\dot{\epsilon}_{ij} = \dot{\epsilon}_{ij}^e + \dot{\epsilon}_{ij}^{vp} \quad (1)$$

The viscoplastic strain is calculated from the following equation:

$$\dot{\epsilon}_{ij}^{vp} = \Phi \frac{\partial f}{\partial \sigma_{ij}} \quad (2)$$

$$\tilde{f} = (\bar{p} - \bar{p}_0) \left[\bar{p} + \frac{R-2}{R} \bar{p}_0 \right] + (R-1)^2 \left(\frac{\bar{q}}{M} \right)^2 = 0 \quad (3)$$

Where the parameter Φ is calculated from the compatibility conditions.

Three surfaces are used in this framework: 1- Reference yield surface ($\tilde{f} = 0$): The yield surface that determines the state of the sample at the reference time (\bar{t}). The definition of such a surface is to obtain the state of the soil sample at the required time (t).

2- yield surface under loading ($\hat{f} = 0$): A surface that contains the stress state.

3-Potential surface ($\hat{\hat{f}} = 0$): The surface that determines the path and rate of strain. ($\hat{\hat{f}}$) can be greater or smaller than (\hat{f}). These three yield surfaces have the same formula but their sizes are different.

The location of the surface with the horizontal axis is the parameter that determines the size of each surface (Figure 1). This parameter is equal to (P_L) for the loading yield surface and the reference yield surface is (\bar{P}_0) and for the potential surface is (\hat{P}_0).

The value of (P_L) changes as a result of loading, but the (\hat{P}_0) value changes with time. Assuming that the

sample is under stable loading, (\hat{p}_0) increases with time. This increase causes a viscoplastic strain in the model. The (\bar{p}_0) value is calculated from the following equation:

$$e = e_N - \lambda \text{Ln}(p_0) + \kappa \text{Ln}(p_0/p) \quad (4)$$

Where (e_N) is the amount of porosity at $(p_0 = 1)$ and at the reference time of (\bar{t}) and (λ) and (κ) are the isotropic consolidation line gradients in the loading and unloading state, respectively.

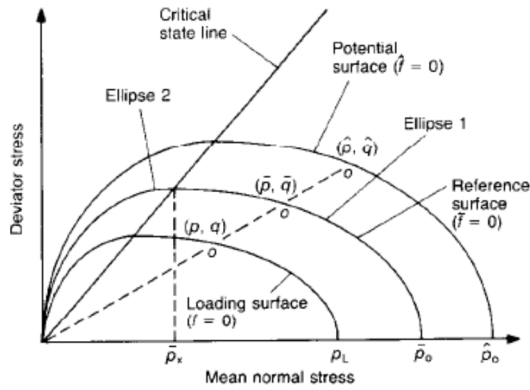


Figure 1. Loading yield and reference yield surfaces and potential surface

The relationship between \hat{p}_0 and \bar{p}_0 is calculated from the following formula:

$$\hat{p}_0 = \bar{p}_0 \left(\frac{\sqrt{(\dot{\varepsilon}_{ij}^{vp})}}{\sqrt{(\bar{\varepsilon}_{ij}^{vp})}} \right)^{\alpha/(\lambda-\kappa)} \quad (5)$$

Where $\dot{\varepsilon}_{ij}$ is the loading strain rate and $\bar{\varepsilon}_{ij}^{vp}$ the viscoplastic strain rate, $\alpha = C_\alpha / \text{Ln}(10)$ and C_α are the index of secondary soil compaction. The value Φ is calculated using the following equation:

$$\Phi = \frac{\alpha_0}{\bar{t}(1+e_0) \left(\frac{\partial \hat{f}}{\partial \hat{p}} \right)_0} \left(\frac{p_L}{\bar{p}_0} \right)^\alpha \quad (6)$$

Where α_0 is the α value obtained in the one-dimensional consolidation test and $\left(\frac{\partial \hat{f}}{\partial \hat{p}} \right)_0$ is the vector perpendicular to the potential surface in the stress path.

$$\Delta \varepsilon_{ij}^{vp} = \Delta t \dot{\varepsilon}_{ij}^{vp} + \theta \Delta t H \sigma \quad (7)$$

$$\Delta \sigma_{ij} = D^e (\Delta \varepsilon_{ij} - \Delta \varepsilon_{ij}^{vp}) \quad (8)$$

1.2. Microplane formulation

The Virtual work performed by stress on the sphere volume of a per-unit radius can be obtained from the stress multiplier integral in the strain development.

$$\delta \dot{W} = \int_V \dot{\sigma}_{ij} \delta \varepsilon_{ij} \quad (9)$$

In the above relation $\delta \varepsilon_{ij}$ is the strain tensor and $\dot{\sigma}_{ij}$ is the stress tensor. The strain vector $d\varepsilon_n$ (can be divided into any plane by the perpendicular to the strain ($d\varepsilon_N$) and the tangent to the plane ($d\varepsilon_T$).

$$d\varepsilon_n = d\varepsilon_N + d\varepsilon_T \quad (10)$$

$$(d\varepsilon_n)_i = n_k d\varepsilon_{ik} \quad (11)$$

$$(d\varepsilon_N)_i = n_i n_j n_k d\varepsilon_{jk} \quad (12)$$

$$(d\varepsilon_T)_i = (n_k \delta_{ij} - n_i n_j n_k) d\varepsilon_{jk} \quad (13)$$

n_i is the vector components perpendicular to the plane and δ_{ij} is the function of the delta kronker. Using the principle of virtual work, we can find the following relation for virtual work in terms of stress and strain components that are depicted on the desired plane:

$$\delta \dot{W} = \frac{4\pi}{3} \dot{\sigma}_{ij} \delta \varepsilon_{ij} = 2 \int_A (\dot{\sigma}_N \delta \varepsilon_N + \dot{\sigma}_T \delta \varepsilon_T) dA \quad (14)$$

Where A is the hemisphere surface with a unit radius, $\dot{\sigma}_N$ is the perpendicular stress vector and $\dot{\sigma}_T$ is the tangential stress vector. If there is a Constitutive relationship between stress and strain, the following relationships can be rewritten for stress with the strain depicted on the plane:

$$\dot{\sigma}_N = D_{NN}^{ep} \dot{\varepsilon}_N + D_{NT}^{ep} \dot{\varepsilon}_T \quad (15)$$

$$\dot{\sigma}_T = D_{TN}^{ep} \dot{\varepsilon}_N + D_{TT}^{ep} \dot{\varepsilon}_T \quad (16)$$

By applying relations 15 and 16 in relation 14 we will have:

$$\dot{\sigma}_{ij} \delta \varepsilon_{ij} = \frac{3}{2\pi} \int_A [(D_{NN}^{ep} \dot{\varepsilon}_N + D_{NT}^{ep} \dot{\varepsilon}_T) \delta \varepsilon_N + (D_{TN}^{ep} \dot{\varepsilon}_N + D_{TT}^{ep} \dot{\varepsilon}_T) \delta \varepsilon_T] dA \quad (17)$$

Deriving the perpendicular and tangential strain of the plane to the strain tensor, the following equations are obtained.

$$\frac{\partial \varepsilon_N}{\partial \varepsilon_{ij}} = n_i n_j = A_{ij}, \quad \frac{\partial \varepsilon_T}{\partial \varepsilon_{ij}} = \frac{n_j n_r}{\varepsilon_T} (\varepsilon_{ir} - n_i n_s \varepsilon_{rs}) = B_{ij} \quad (18)$$

By placing relation 18 in relation 17, the stress-strain Constitutive model is obtained in the Microplanes framework.

$$\dot{\sigma}_{ij} = \frac{3}{2\pi} \int_A [(D_{NN}^{ep} A_{rs} + D_{NT}^{ep} B_{rs}) A_{ij} + (D_{TN}^{ep} A_{rs} + D_{TT}^{ep} B_{rs}) B_{ij}] \dot{\varepsilon}_{rs} dA \quad (19)$$

A finite number of integration points can be used to estimate the relation 19, using the Gaussian numerical integral. These integration points are compatible with a limited number of Microplanes. Table 1 shows the unit vectors perpendicular to the planes and the weighting coefficients of integration. Using the numerical integral, the following relation can be used to determine the stress:

$$\dot{\sigma}_{ij} = 6 \sum_{\beta=1}^n w_\beta (D_{ijrs}^{ep})_\beta (\dot{\varepsilon}_{rs})_\beta \quad (20)$$

$$\left(D_{ijrs}^{ep} \right)_\beta = \left[\left(D_{NN}^{ep} A_{rs} + D_{NT}^{ep} B_{rs} \right) A_{ij} + \left(D_{TN}^{ep} A_{rs} + D_{TT}^{ep} B_{rs} \right) B_{ij} \right]_\beta \quad \text{Where } n_1 \text{ is the first component of the perpendicular vector on the plane, } q \text{ and } p \text{ are the stress invariants. A similar relation can also be given for strain:}$$

(21)

1.3. Applying elasto-viscoplastic Constitutive model in Microplane framework

Table 1. Perpendicular vector and weight ratio of plane integration

Plane No	normal axis			Plane No	normal axis			W _i
	n ₁	n ₂	n ₃		n ₁	n ₂	n ₃	
1	$\frac{\sqrt{3}}{3}$	$\frac{\sqrt{3}}{3}$	$\frac{\sqrt{3}}{3}$	2	$\frac{\sqrt{3}}{3}$	$-\frac{\sqrt{3}}{3}$	$\frac{\sqrt{3}}{3}$.020277 985
3	$-\frac{\sqrt{3}}{3}$	$\frac{\sqrt{3}}{3}$	$\frac{\sqrt{3}}{3}$	4	$-\frac{\sqrt{3}}{3}$	$-\frac{\sqrt{3}}{3}$	$\frac{\sqrt{3}}{3}$.020277 985
5	$\frac{\sqrt{2}}{2}$	$\frac{\sqrt{2}}{2}$	0	6	$-\frac{\sqrt{2}}{2}$	$\frac{\sqrt{2}}{2}$	0	.058130 468
7	$\frac{\sqrt{2}}{2}$	0	$\frac{\sqrt{2}}{2}$	8	$-\frac{\sqrt{2}}{2}$	0	$\frac{\sqrt{2}}{2}$.030091 134
9	0	$-\frac{\sqrt{2}}{2}$	$\frac{\sqrt{2}}{2}$	10	0	$\frac{\sqrt{2}}{2}$	$\frac{\sqrt{2}}{2}$.030091 134
11	1	0	0	12	0	1	0	.038296 881
13	0	0	1	-	-	-	-	.029390 060
14	$\frac{\sqrt{6}}{6}$	$\frac{\sqrt{6}}{6}$	$\frac{\sqrt{2}}{\sqrt{3}}$	15	$\frac{\sqrt{6}}{6}$	$-\frac{\sqrt{6}}{6}$	$\frac{\sqrt{2}}{\sqrt{3}}$.019070 616
16	$-\frac{\sqrt{6}}{6}$	$\frac{\sqrt{6}}{6}$	$\frac{\sqrt{2}}{\sqrt{3}}$	17	$-\frac{\sqrt{6}}{6}$	$-\frac{\sqrt{6}}{6}$	$\frac{\sqrt{2}}{\sqrt{3}}$.019070 616

In this section, Pastor-Zienkiewicz Constitutive model is implemented in the Microplane framework. Defined equations in Constitutive models use stress and strain variables. Therefore, the equations needed to calculate stress and strain depicted on each page from the invariant stress and strain values.

Using the definitions of the perpendicular and tangent components of the stress on the plane, the following relation is obtained:

$$\begin{bmatrix} d\sigma_N \\ d\sigma_T \end{bmatrix} = \begin{bmatrix} 1 & n_1^2 - 1/3 \\ 0 & n_1 \sqrt{1 - n_1^2} \end{bmatrix} \begin{bmatrix} dp' \\ dq \end{bmatrix} = \mathbf{E} \begin{bmatrix} dp' \\ dq \end{bmatrix}$$

(22)

$$\begin{bmatrix} d\varepsilon_N \\ d\varepsilon_T \end{bmatrix} = \begin{bmatrix} 1/3 & 1.5(n_1^2 - 1/3) \\ 0 & 1.5n_1 \sqrt{1 - n_1^2} \end{bmatrix} \begin{bmatrix} d\varepsilon_v \\ d\varepsilon_s \end{bmatrix} = \mathbf{F} \begin{bmatrix} d\varepsilon_v \\ d\varepsilon_s \end{bmatrix}$$

(23)

Using the Pastor-Zienkiewicz Constitutive Model, the following relation can be presented for plastic strain on plates:

$$\begin{bmatrix} d\sigma_N \\ d\sigma_T \end{bmatrix}_{LU} = \begin{bmatrix} D_{NN}^e & D_{NT}^e \\ D_{TN}^e & D_{TT}^e \end{bmatrix} \begin{bmatrix} d\varepsilon_N - d\varepsilon_N^{vp} \\ d\varepsilon_T - d\varepsilon_T^{vp} \end{bmatrix} = D^e \begin{bmatrix} d\varepsilon_N \\ d\varepsilon_T \end{bmatrix}$$

(24)

By assigning stress and strain from equations 22 and 23 to equation 24, the strain and stress invariants on each plane can be related. In the following equation, the plane number is shown with the subscript i.

$$\begin{bmatrix} dp' \\ dq \end{bmatrix}_i = E_i^{-1} \times (D^e)_i \times F_i \times \begin{bmatrix} d\varepsilon_v^e \\ d\varepsilon_s^e \end{bmatrix}_i$$

(25)

The total stress development can be calculated by placing the equation 25 in equation 20.

$$\begin{bmatrix} dp' \\ dq \end{bmatrix}_i = 6 \sum_{i=1}^n w_i \left(A_i^{-1} \times (D^e)_i \times B_i \times \begin{bmatrix} d\varepsilon_v^e \\ d\varepsilon_s^e \end{bmatrix}_i \right)$$

(26)

1.4. Numerical Modeling

Figures (2) to (9) present the results of modeling performed on normal consolidated soil (Liu et al, 2018). These tests are performed at the strain rates of .00078 % / min and 1% / min . The parameters used in this modeling are as follows:

Table 2. Parameters used in modeling

λ	κ	M	ν	e_N	$C_{\alpha 0}$
.151	.018	1.25	.3	1.515	.0139

As shown in Figures 2 and 3, the modeling results are in good agreement with the experimental results.

As the strain rate increases, the constitution of the consolidated normal soil will be similar to that of the pre-consolidated soil.

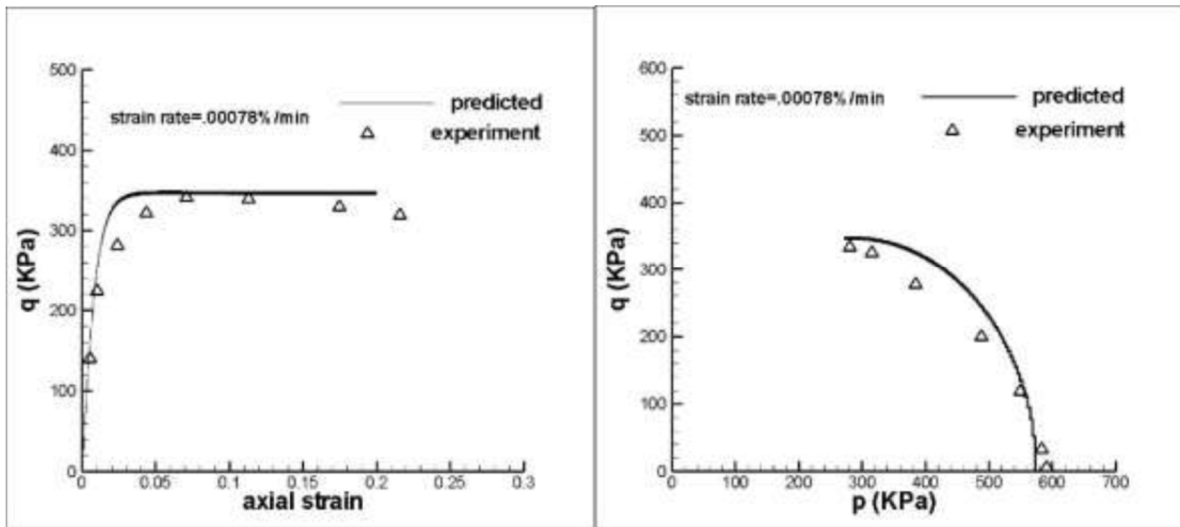


Figure 2. Results of a non-drained triaxial test with strain rate of .00078 % / min
 (a) Stress path (b) Axial strain- deviator stress

Figures 4 and 5 illustrate the variations of the deviator stress, bulk stress and pore water pressure over time. Stress changes increase in early times and decrease over time. In addition, by increasing the strain rate (1% / min), the pore water pressure initially increases and decreases at the end of the test, which indicates constitution similar to pre-consolidated clay. However, for the low strain rate, the pore water pressure increases steadily and then remain constant.

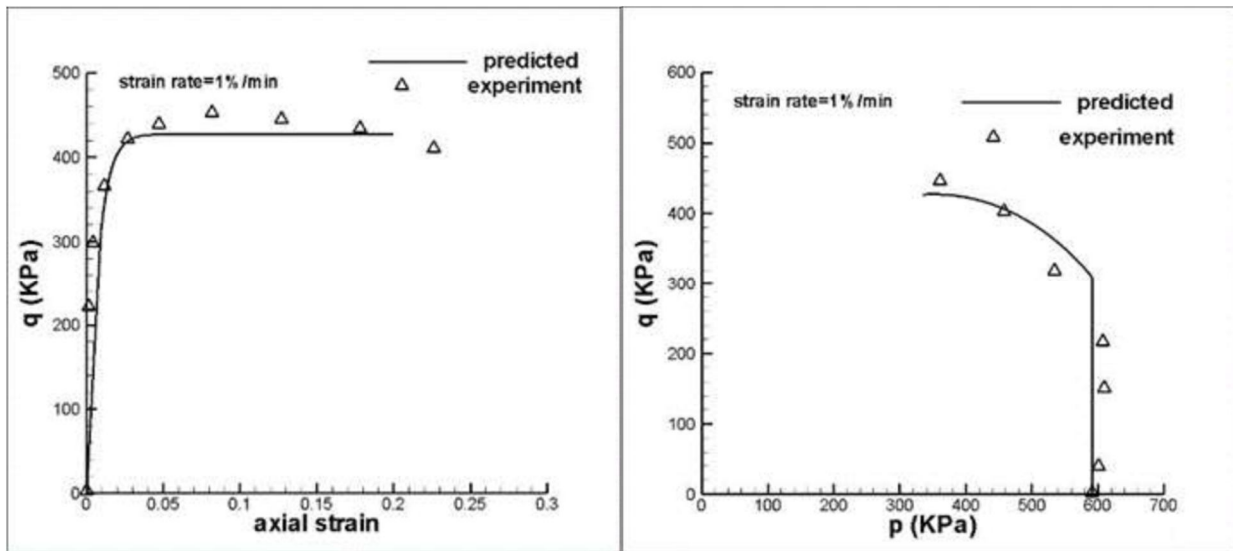


Figure 3. Results of a non-drained triaxial test with strain rate of 1% / min
 (a) Stress path (b) Axial strain- deviator stress

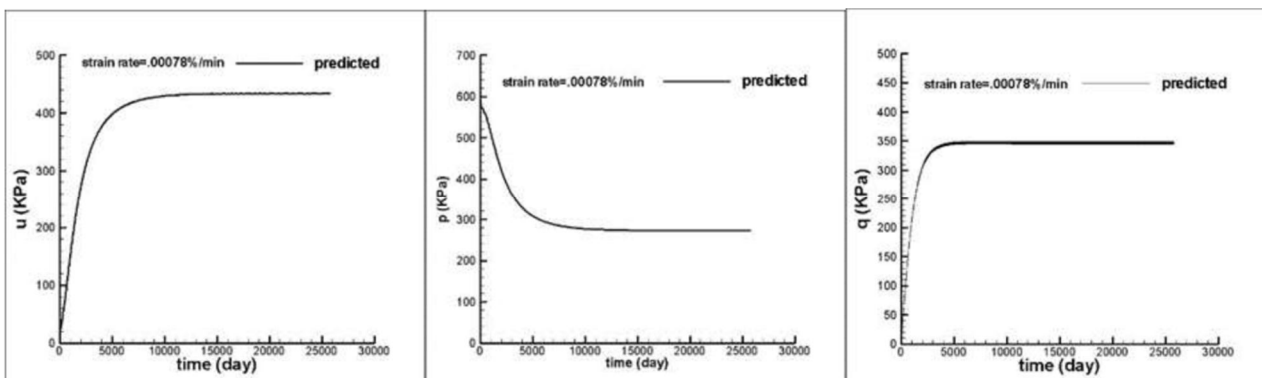


Figure 4. Variations (a) Deviator stress (b) Bulk stress (c) Pore water pressure over time for Non-drained triaxial test with strain rate of .00078%/ min .

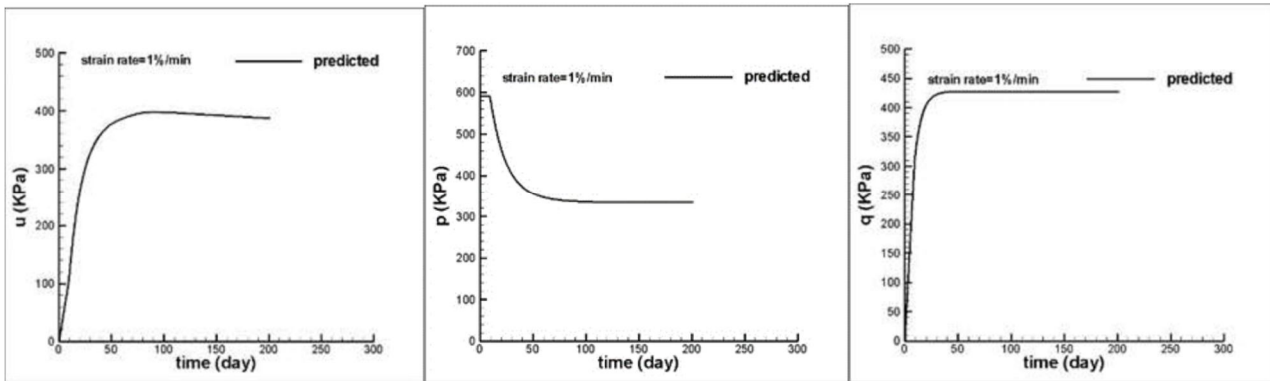


Figure 5. Variations (a) Deviator stress (b) Bulk stress (c) Pore water pressure over time for Non-drained triaxial test with strain rate of 1%/ min .

Figures 6 and 7 illustrate the changes in normal stress relative to normal strain. The normal stress on planes 5,6,7 and 8 shows a maximum value as the strain rate increases. Using Figures 8 and 9, it can be concluded that the maximum shear stress on planes 5,6,7 and 8 is more likely due to the local strain on these planes.

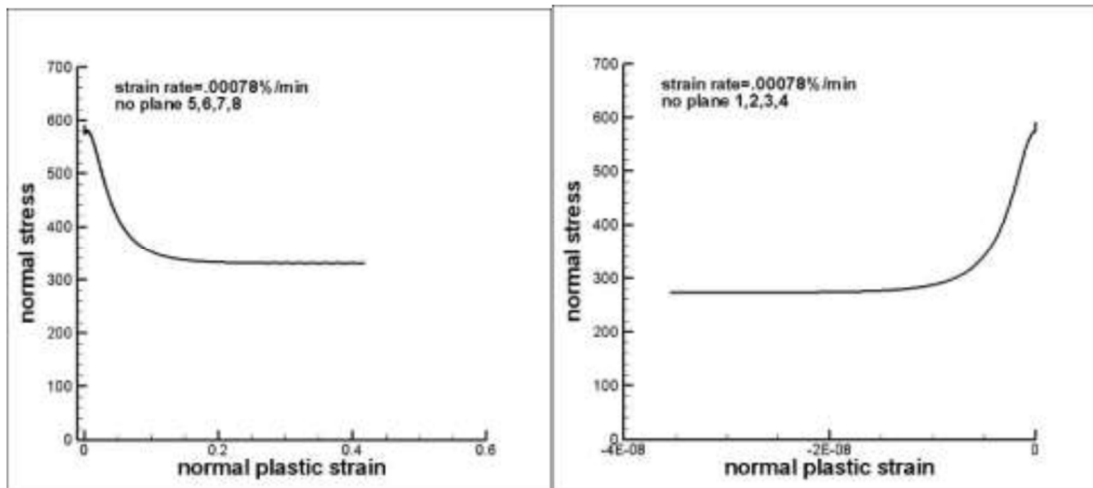


Figure 6. Normal stresses generated on different planes for non-drained triaxial test with strain rate of .00078 % / min .

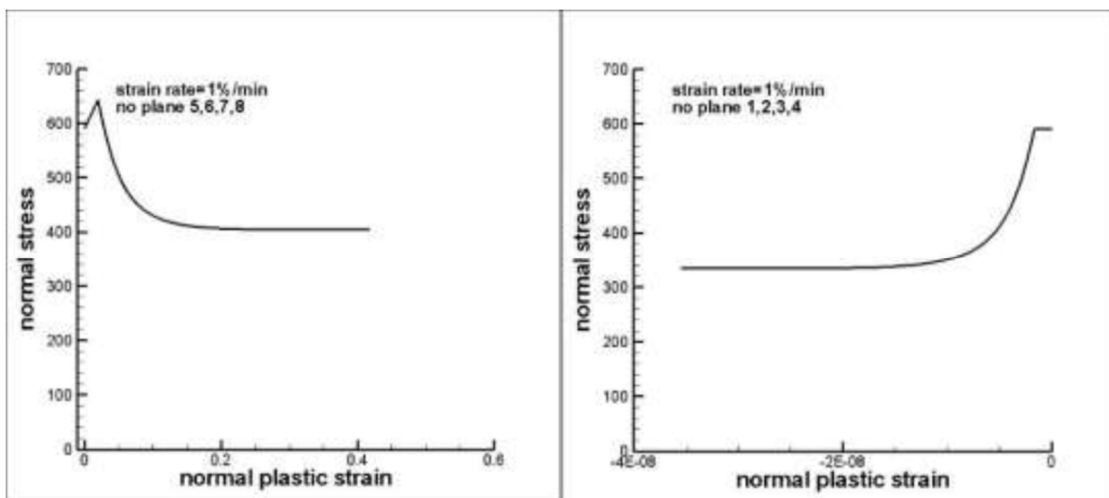


Figure 7. Normal stresses generated on different planes for non-drained triaxial test with strain rate of 1%/ min .

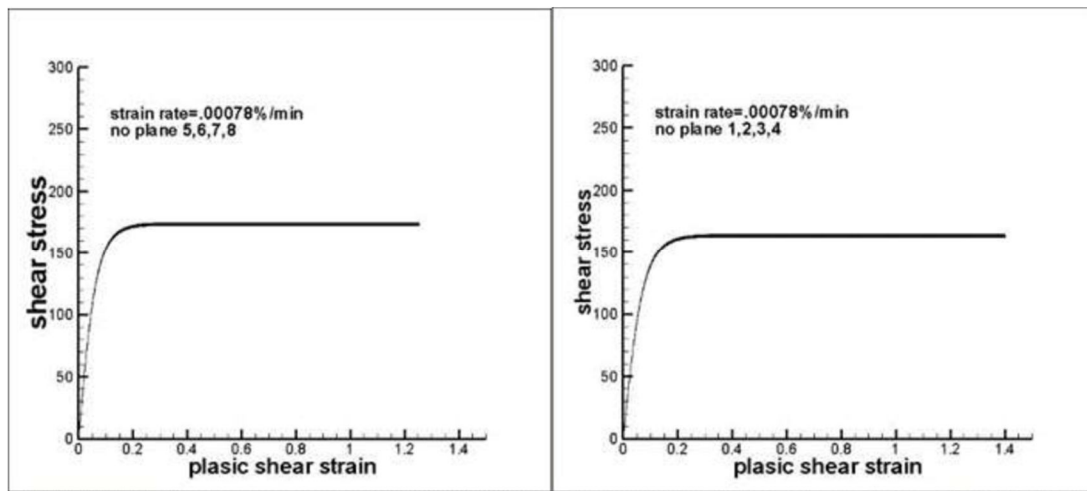


Figure 8. Normal stresses generated on different planes for non-drained triaxial test with strain rate of $.00078\% / \text{min}$.

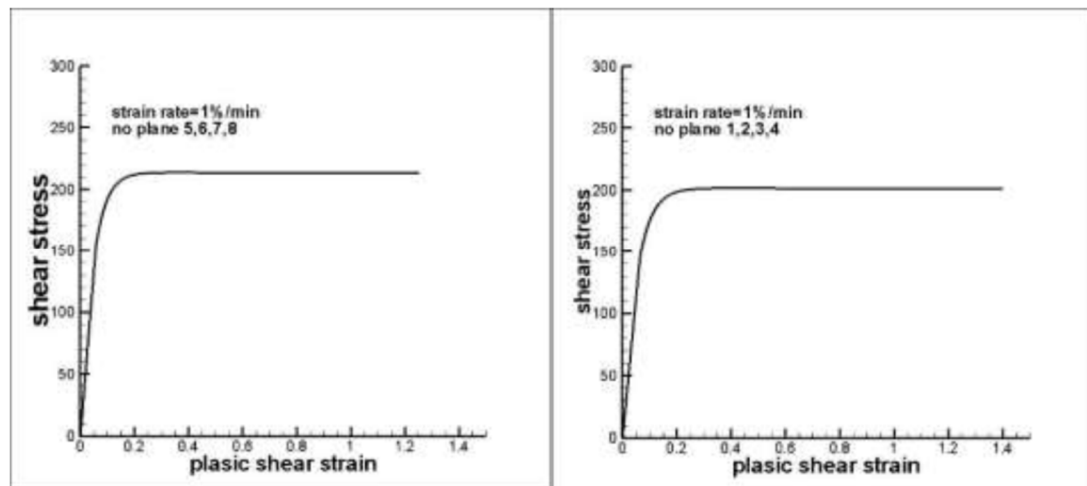


Figure 9. Normal stresses generated on different planes for non-drained triaxial test with strain rate of $1\% / \text{min}$.

2. CONCLUSION

A constitutive model was presented to describe the mechanical behavior of the clay. This constitutive model was created by applying an elasto-viscoplastic constitutive model in the Microplane framework. The proposed model is capable of depicting behavior on planes within the material. we can detect failure mechanisms with this feature. The angles of fracture planes are determined with using this model. In addition, the constitutive dependence of material to time can also be modeled well. Briefly, the presented model has the advantages of both constitutive models.

REFERENCES

- [1] Adachi, Liu, C., Shanthraj, P., Diehl, M., Roters, F., Dong, S., Dong, J., Raabe, D. (2018). An integrated crystal plasticity–phase field model for spatially resolved twin nucleation, propagation, and growth in hexagonal materials. *International Journal of Plasticity*, 106, 203-227.
- [2] P. Shanthraja, B. Svendsena, L. Sharmaa, F. Rotersa, D. Raabe, Elasto-viscoplastic phase field modelling of anisotropic cleavage fracture, *Journal of the Mechanics and Physics of Solids*, 99 (2017) 19–34.
- [3] Pham, K., Amor, H., Marigo, J.-J., Maurini, C., 2011. Gradient damage models and their use to approximate brittle fracture. *Int. J. Damage Mech.* 20 (4, SI), 618–652.
- [4] Batdorf SB, Roters, F., Diehl, M., Shanthraj, P., Eisenlohr, P., Reuber, C., Wong, S. L., ... & Nikolov, S. (2019). DAMASK–The Düsseldorf Advanced Material Simulation Kit for modeling multi-physics crystal plasticity, thermal, and damage phenomena from the single crystal up to the component scale. *Computational Materials Science*, 158, 420-478.
- [5] Bazant ZP, Gambarova PG.(1984) Crack shear in concrete: Crack band micro plane model, *J. Struct. Eng.*, ASCE, 110: 2015-2036
- [6] Kutter, Teichtmeister, S., Kienle, D., Aldakheel, F., & Keip, M. A. (2017). Phase field modeling of fracture in anisotropic brittle solids. *International Journal of Non-Linear Mechanics*, 97, 1-21.
- [7] Perzyna, P. (1966). Fundamental problems in viscoplasticity. *Adv. Appl. Math.* 9,243-377
- [8] Wu, J. Y., Nguyen, V. P., Nguyen, C. T., Sutula, D., Bordas, S., & Sinaie, S. (2018). Phase field modeling of fracture. *Advances in Applied*

Mechanics: Multi-scale Theory and Computation,
52.

- [9] Diehl, M., Wicke, M., Shanthraj, P., Roters, F.,
Brueckner-Foit, A., & Raabe, D. (2017). Coupled

crystal plasticity–phase field fracture simulation
study on damage evolution around a void: pore
shape versus crystallographic orientation. *JOM*,
69(5), 872-878.